Influence of Energy Dissipation on PWR Fuel Assembly Behaviour During Severe Seismic Excitation

J.-D. Kim, U. Borsdorf, H. P. Fuchs, J. Stabel
Siemens Aktiengesellschaft, Erlangen, FRG

INTRODUCTION

The capability of the control rods to shut down the reactor must be ensured even in the event of a severe earthquake. Since, in a pressurized water reactor, the control rods are moved through guide thimbles located within the fuel assembly, maintenance of shutdown capability requires that any deformation of the spacer grids of the fuel assemblies (FA) loacated in control rod positions must not exceed permissible limits. For reasons of neutron physics, however, no control assemblies are located in the outermost core zone. So to get sufficient information on shutdown capability it is necessary to gather precise information on loads of the spacer grids, the dagree of the deformation of the spacer grids and the distribution of both within the core if the spacer grid buckling limit is exceeded locally as a result of the loads occuring under severe earthquake conditions. For realistic results the dissipation of energy in the spacer grids and cumulative increase in gap size which result from the elastoplastic deformation of the spacer grid have to be considered.
For the following study a certain shutdown earthquake was selected and the intensity was increased by a factor of 2 and 3 to show the influence of energy dissipation on spacer grid load and deformation.

FUEL ASSEMBLY MODEL, CORE MODEL AND METHOD

A row model consisting of 13 individual FAs separated from one another and from the core shroud by distances equal to the gaps in the actual core was selected to represent the core for the structural dynamic investigation (Figure 1).
Each FA was simulated by massless beam elements and by nodes over which the FA masses were distributed proportionally. Spring elements with gap were arranged at the various spacer grid levels and connected in series with linear tension/compression spring to represent adequately realistic one- and two-sided impacts. This FA calculation model has been verified in extensive tests (Kim et al, 1981). The nonlinear spring for the two-sided impact (Fig.2) which accounts fore the gap between neighbouring FA's, the elastic behaviour before buckling and the plastic post buckling behaviour is an idealized spring characteristic determined on a statistical basis from static spacer grid buckling tests. When the spacer grid is loaded up to the point 4 and in the following unloaded, for example, an additional gap 1-5 is created and an energy dissipation 1-2-3-6-5 results. When the loading is then increased to 6 and then unloaded to 7, a total plastic gap 1-7 is generated and a energy dissipation 5-4-6-7 results.

All dynamic interactions within the vibrating system were calculated with the KWUSTOSS computer code.
KWUSTOSS is a development of SIEMENS with the following characteristics:
- nonlinear dynamic code
- explicit, implicit or coupled explicit-implicit schemes of integration
- consideration of post buckling behaviour of spacers
- specialized fluid-structure interaction
- various damping mechanisms

CALCULATION CASES

For the parametric study two typical seismic events with different frequency content were selected (type A: hard soil, type B: soft soil). The corresponding motion, resulting from an analysis of building- and primary-circuit-structure, were applied to grid plate of the upper core structure, core shroud and lower core support plate. The acceleration response spectra at 3 % damping for the two earthquakes are shown for the grid plate in fig. 3 as an example.
Table 1 shows the paramter studies carried out:
The excitation intensities used in the parameter study were obtained by increasing the intensity of the safe shutdown earthquake by a factor of 2 and 3 respectively. Both the elastic and elastoplastic analyses were performed using the time history method.

Type of excitation		Type A		Type B	
Method of analysis		elast.	elastoplast.	elast.	elastoplast.
	SSE	+		+	+
Excitaion	x 2	+	+	+	+
Intensity	x 3	+	+	+	+

Table 1: Calculation cases

RESULTS

The time history curves at double the SSE excitation intensity for deflection at the 5th spacer grid, which is located at half the FA height, are shown in
- Figure 4a for type B - elastic analysis
- Figure 4b for type A - elastic analysis
- Figure 4c for type B - elastoplastic analysis with an assumed spacer grid buckling limit of 20 KN.

The dominant low-frequency and hign-frequency components of the forced FA vibrations can be clearly seen in Figures 4a and 4b. When the spacer grid buckling limit is exceeded, the plastic deformation which occurs causes a marked increase in FA deflection (Figures 4a and 4c).

The maximum impact forces and plastic deformations at the spacer grids of each FA found for the various excitation intensities in the elastic and elastoplastic analyses are shown in Figure 5 for type A earthquake and in Figure 6 for type B respectively. If the maximum spacer grid impact force (elastic analysis) is plotted against the excitation intensity (Figure 7), it becomes apparent that the increase in impact force with increasing excitation intensity is not as sharp for type B (soft soil) as for type A (hard soil). On the other hand, type B exhibits a sharper increase in spacer grid deformation (elastoplastic analysis) with increasing excitation intensity than does type A (Figure 5 and 6). Under low-frequency excitation, the vibrating system apparently has more time to respond to the input motion with increasing plastic deformation.

The maximum spacer grid deformations at **control assembly positions** for the excitation intensities used were:

Earthquake	Type A	Type B
Reference case (SSE)		< 1 mm
SSE x 2	< 1 mm	3.0 mm
SSE x 3	< 4.0 mm	3.6 mm

Tests have demonstrated that the position of the guide thimbles within the spacer grid changes only when plastic spacer grid deformation reaches approximately 3 mm. Since the control rods of a PWR are individually guided in the FA guide thimbles, the maximum permissible spacer grid deformation still allowing proper CA function actually exceeds this number. A further margin of spacer grid deformation is available before the ovalisation of guide thimbles begins to impede CA function.

CONCLUSIONS

The conclusions drawn from the calculations described here are as follows:

- The spacer grid loadings and deformations increase with increasing excitation intensity, but differently depending on whether the excitation is of low or high frequency.
- The maximum spacer grid loadings and deformations on each fuel assembly occurred at half the fuel assembly height.
- The maximum spacer grid loadings and deformations within the core occurred at the core periphery.
- In case of elastic analysis the spacer grid loads were over the whole core nearly as high as at the core periphery.
- The elastoplastic analysis showed that due to energy dissipation resulting from buckling of the peripheral spacer grids the loads in the center markedly decreased.

Summarizing the results of the study it is obvious that for the case that spacer grid loading exceeds the buckling limit at any point within the core, the dynamic structural behaviour of the FAs can be described only by means an elastoplastic analysis.

REFERENCE

Kim J.-D., Borsdorf U. and Stern G. (1981). Comparison of Theoretical and Experimental Examinations of PWR Fuel Assemblies under External Loads. Transactions of the 6th International Conference on SMIRT, Vol.C.

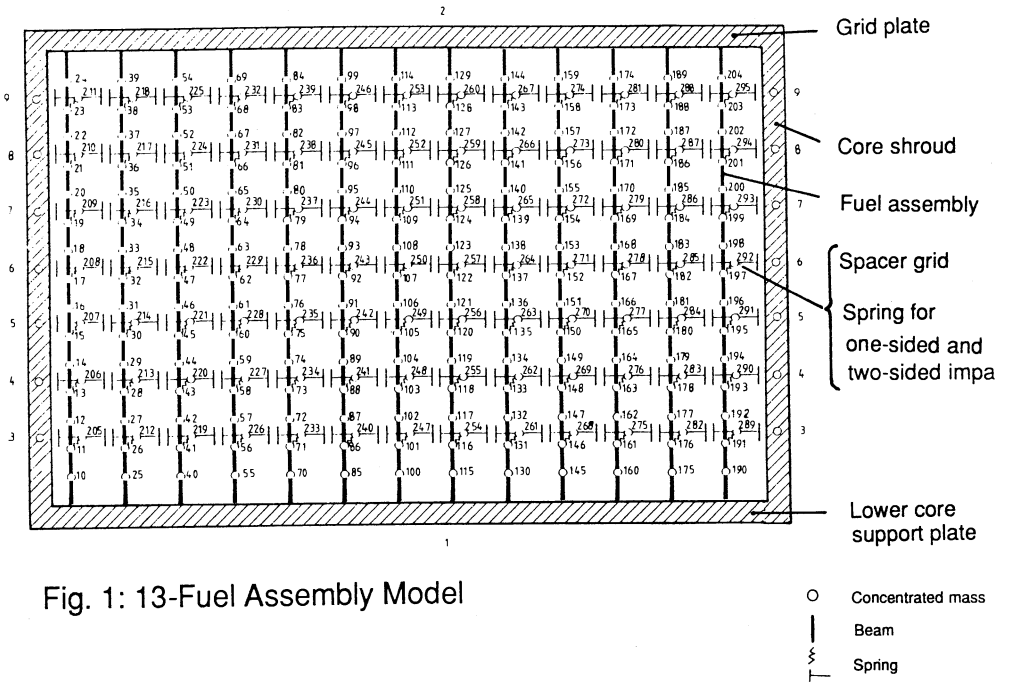

Fig. 1: 13-Fuel Assembly Model

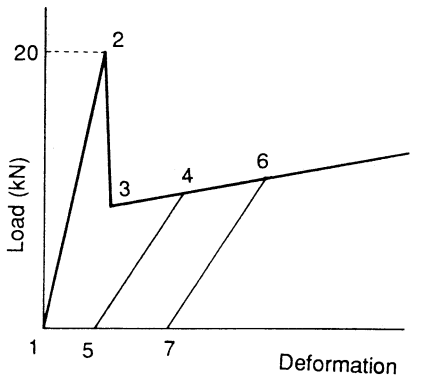

Fig. 2:
Spacer Grid Characteristic

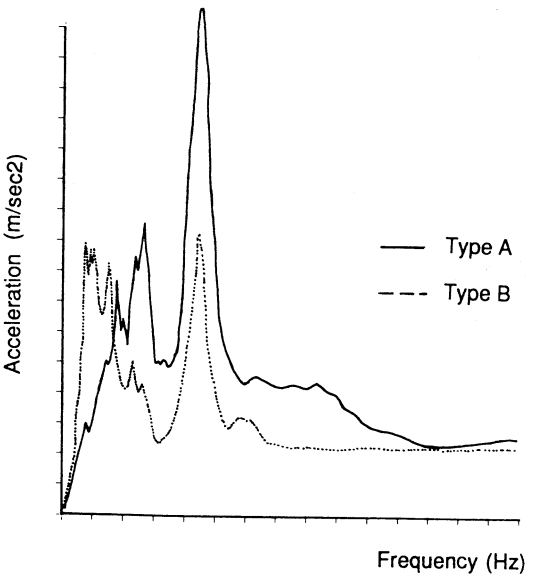

Fig. 3:
Safety Shutdown Earthquake
Response Spectra on the Grid Plate

Fig. 4: Fuel Assembly Displacements and Loads to the Core Shroud (5-th Spacer Grid)

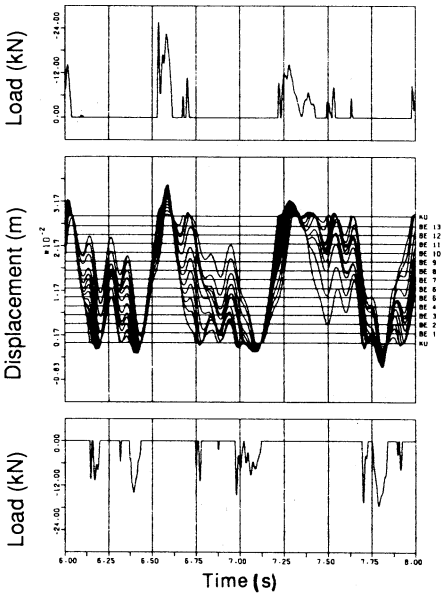

Fig. 4a: Elastic Analysis
Excitation Type B
(2 x SSE)

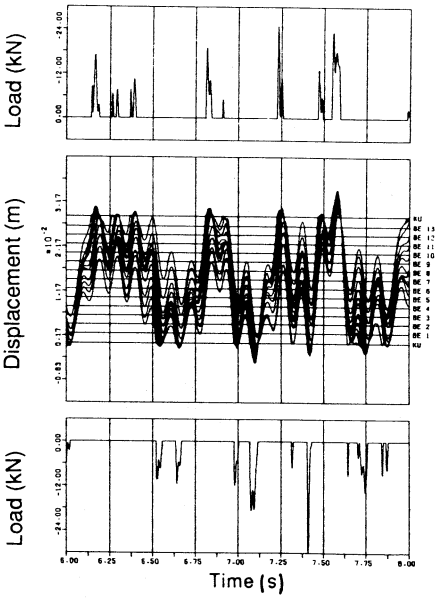

Fig. 4b: Elastic Analysis
Excitation Type A
(2 x SSE)

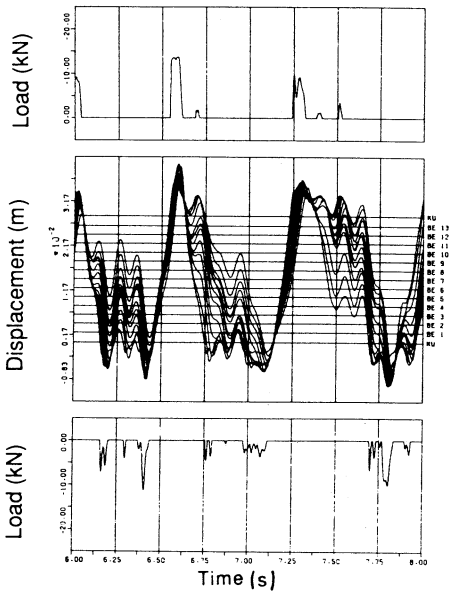

Fig. 4c: Elastoplastic Analysis
Excitation Type B
(2 x SSE)

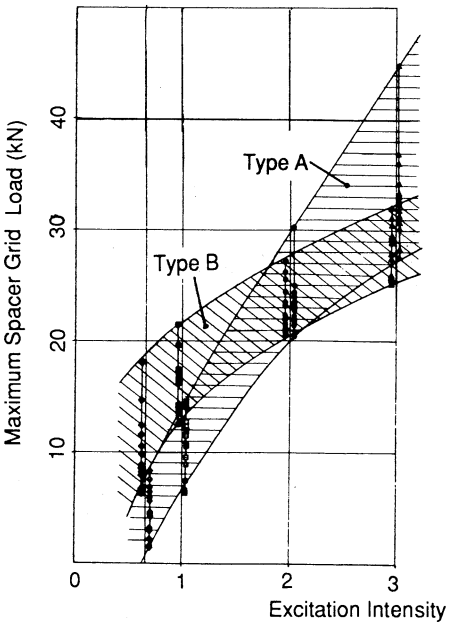

Fig. 7: Maximum Spacer Grid Impact Load of the Individual Fuel Assemblies

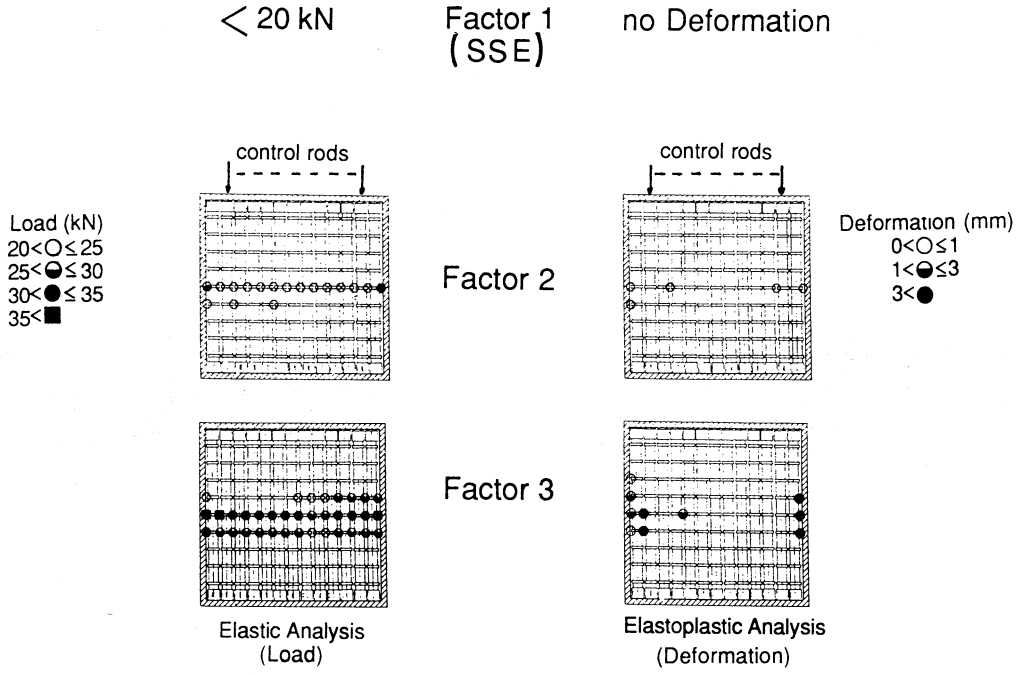

Fig. 5: Maximum Spacer Grid Impact Load and Deformation for the Excitation Type A

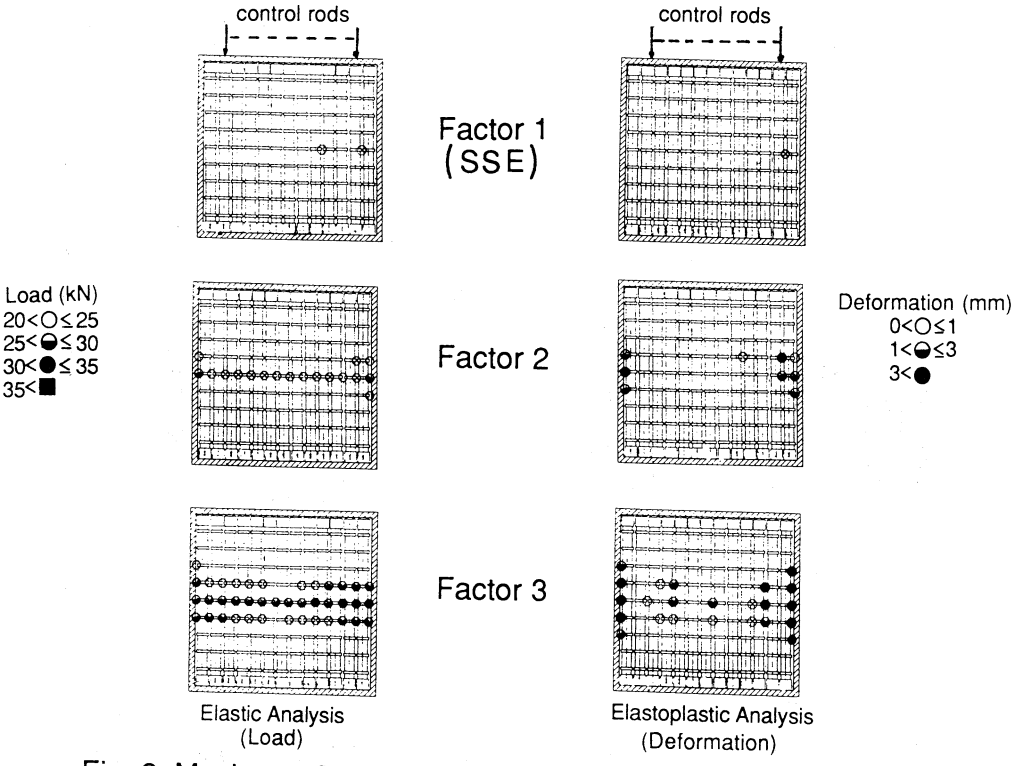

Fig. 6: Maximum Spacer Grid Impact Load and Deformation for the Excitation Type B